ACS APPLIED ELECTRONIC MATERIALS

pubs.acs.org/acsaelm Article

Application of a Bio-Nanocomposite Tissue as an NIR Optical Receiver and a Temperature Sensor

Giovanni Landi* and Heinz-Christoph Neitzert

Cite This: *ACS Appl. Electron. Mater.* 2021, 3, 2790−2797 Read Online

ACCESS | Metrics & More | Article Recommendations | Supporting Information

ABSTRACT: The application of a type of bio-nano tissue, consisting of tobacco cells and multiwalled carbon nanotubes, as a sensitive near-infrared region (NIR) bolometer operating at room temperature was investigated. An electrical resistor-type sensor was fabricated by the evaporation of lateral gold contacts. A very low dark conductivity was achieved by a high-voltage treatment of a strongly conducting nanotube network. Although before the treatment the electrical transport was dominated by the percolative transport in the nanotube network, after the voltage stress the electronic transport in the low-conductivity tissue was controlled only by the intrinsic electrical properties of the biological matrix. In this latter case, the conductivity was extremely temperature and humidity dependent. However, on operating the sensor tissue in a small temperature window around room temperature, the change in humidity could be neglected. Under these conditions, the multifunctional device functioned as a very high sensitivity temperature sensor with a temperature coefficient of resistance of more than −20%/K. Sensitive bolometer operation with a very good signal-to-noise ratio was demonstrated by irradiation of the tissue with low-power LEDs in the near-infrared range between 780 and 1720 nm.

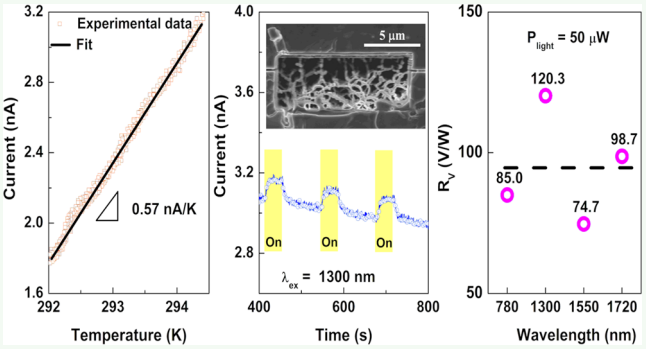

KEYWORDS: *carbon nanotubes, nanocomposites, temperature sensor, NIR bolometer, bio-nano tissue*

INTRODUCTION

Multifunctional sensors have attracted increasing interest owing to their ability to detect different physical parameters, such as pressure, strain, temperature, humidity, light, and chemical compounds, simultaneously in one detection unit.[1] These sensors have a wide range of applications in the fields of robotics and artificial skins, smart building and energy efficiency, optical communications and light detection, biomedical and remote environmental sensing, autonomous driving, etc.[2,3] To date, such devices have been fabricated using complex and expensive processes requiring deposition conditions and device packaging in vacuum using inorganic materials (e.g., rare earth elements, semiconductors, and superconductors).[4−7]

In the last few decades, many authors have reported multifunctional sensors fabricated with alternative low-cost sensing materials and easier fabrication processes based on polymers and organic compounds combined with different fillers (e.g., carbon black, carbon nanotubes, graphene, molybdenum disulfide, etc.).[8,9] For example, Tsang et al. described a multifunctional composite sensor, based on polymers and porous carbon, having the capability to sense pressure and temperature simultaneously for health monitoring.[8] Moreover, Kim et al. reported a platform with multisensing functions that responds to various stimulations, including weak gas (air) flow, direct physical touch, light, and heat, based on organic field-effect transistors with polymer-dispersed liquid crystals.[9] More recently, several studies have described complete electronics systems (e.g., sensors, complementary inverters, and energy storage devices) based on biodegradable and environmentally friendly materials.[10−13]

In the present study, a biodegradable nanocomposite fabricated with tobacco cells with the addition of multiwalled carbon nanotubes (MWCNTs) has been proposed as a sensing material for a low-cost multifunctional sensor. In this proof of concept, tobacco cells are used as scaffolds to create a biodegradable structure where the conductive carbon nanotubes are confined. The addition of the MWCNTs permits functionalization of the material, making the tissue sensitive to both temperature variations and light in the near-infrared region (NIR). In particular, the device shows a bolometric behavior due to its ultrahigh value of the temperature coefficient of resistance (TCR) observed at room temperature.

Received: April 19, 2021
Accepted: May 6, 2021
Published: May 19, 2021

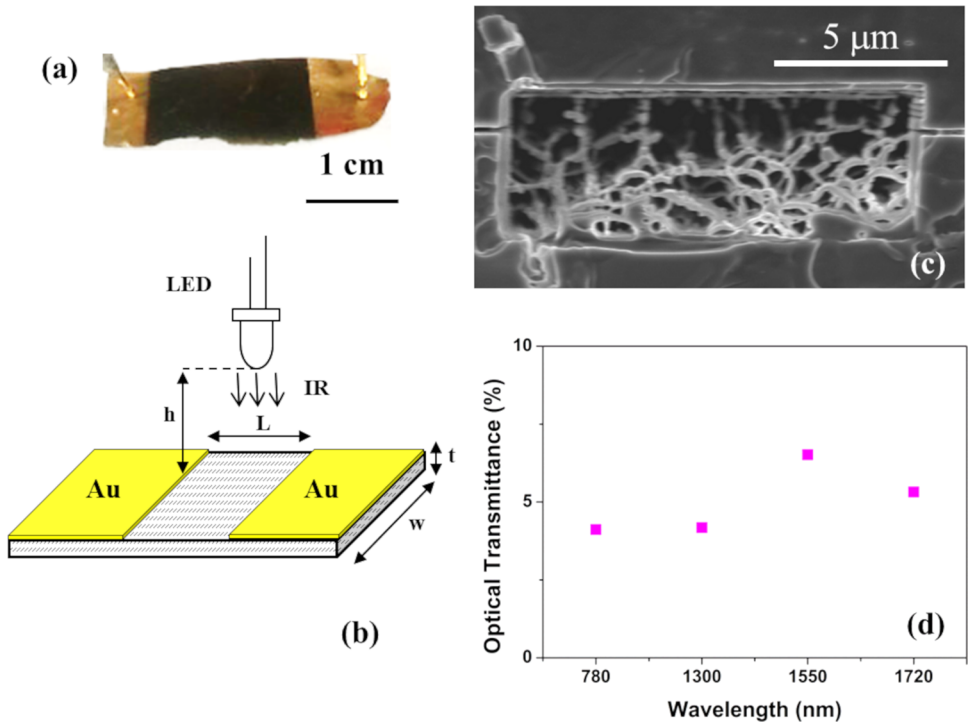

Figure 1. (a) Digital camera picture of the sample during operating conditions with an applied bias voltage. The film has a 2 cm wide and 1 cm long area and a thickness of about 142 μm. (b) Experimental setup used to investigate the unsuspended photosensitive device based on tobacco cells and MWCNTs with coplanar gold contacts. (c) Scanning electron micrograph of the investigated sample after opening with a focused ion beam. (d) Optical transmittance of the thin film measured at telecom wavelengths in the near-infrared region. The incident light power P_{light} is 50 μW.

Here, the electrical output signal of the bolometer, related to the intrinsic properties of the developed tissue, is proportional to the temperature and it does not depend on the device area.[14] A variety of bolometer sensors have been employed for a wide range of applications, such as in night vision systems in automobiles, astronomy, and energy leakage detection tools.[15] To reveal the sensing properties of the bio-nanocomposite tissue, the current−voltage characteristics and the temperature dependence of the material were determined. Moreover, the photoresponse at different light intensities and excitation wavelengths in the NIR wavelength range was evaluated. In addition, the correlation between the temperature variation at the surface and the induced change in the electrical characteristics as a function of light irradiation was analyzed in terms of voltage responsivity, speed response, and thermal boundary conditions of the device.

EXPERIMENTAL SECTION

Sample Preparation. Multiwalled carbon nanotubes (Type "3100" from Nanocyl) were dissolved in distilled water with the help of sodium dodecyl sulfate (SDS) as a surfactant and mixed with tobacco cells from the BY-2 cell line derived from the callus of Nicotiana tabacum seedlings.[16] This cell line is quite easily available and often used as a model system for higher plants. For all details regarding the bio-nano tissue fabrication and its original mechanical and electrical properties, the reader is referred to a previous publication.[17] The final device was fabricated by evaporating lateral gold electrodes on top of the bio-nano tissue. The sample electrical resistance was originally about 3 MΩ. However, after this sample had been exposed for a longer time to a high voltage of 150 V, the conductivity decreased by some orders of magnitude, probably due to the complete interruption of the nanotube percolation path. A photograph of the finished sample is shown in the inset of Figure 1a. The sensitive area of the sample was 1 cm wide (W) and 2 cm long (L) and the average film thickness (t) of the photosensitive tissue without metallization was 142 μm. Here, each electrode was 0.5 cm wide and 1 cm long.

Sample Characterizations. In the investigated sample, the carbon nanotubes could not be detected anymore on the sample surface. Therefore, the sample was opened using a focused ion beam (FIB) instrument with Ga^+ ions to cut a rectangular-shaped window into the sample. The FIB instrument was also equipped with a scanning electron microscope (SEM) for additional imaging of the sample. The current−voltage characteristics (I−V) of the device were measured under dark conditions and under illumination using a Keithley 487 source meter. All presented measurements were performed at room temperature without temperature regulation. The light-emitting diodes (LEDs) were current-biased using a Melles Griot 06DLD103 diode laser controller. This measurement setup is shown in Figure 1b. The LEDs with emission at different wavelengths within the near-infrared (NIR) region (780, 1300, 1550, and 1720 nm) were positioned at a distance of 2.5 cm above the sensitive area of the investigated device. The nominal maximum power of the LEDs was 5mW. The calibration of the incident power at 780 nm was performed using a Hamamatsu S2386 silicon photodiode. The calibration for the LEDs with emitting wavelengths at 1300, 1550, and 1720 nm was done using a Hamamatsu G5832-03 InGaAs photodiode.

The experimental measurements were conducted by applying a constant bias voltage of 10 V to the coplanar contacts with the switching of the infrared light source having a period of about 120 s. Under these operating conditions, the temperature was monitored using a 10 kΩ thermistor with a negative temperature coefficient (NTC). Additionally, the amount of water contained within the sample was monitored by performing gravimetric measurements before and after the measurement cycles using a Sartorius MA-30 moisture analyzer. It should be noted that even after more than 2 years of storage, the investigated film had excellent mechanical properties such as high flexibility. For the as-grown film, the mechanical properties have already been reported in detail.[17] The

https://doi.org/10.1021/acsaelm.1c00368
ACS Appl. Electron. Mater. 2021, 3, 2790−2797

surface temperature was monitored with a FLUKE 576 high-precision infrared thermometer.[18]

RESULTS AND DISCUSSION

The SEM image of the investigated sample is shown in Figure 1c. Here, the carbon nanotube (CNT) bundles are observed to be distributed around the tobacco cells that act as a scaffold. This leads to the formation of a porous film structure, where the MWCNTs form a conductive network. This network is clearly seen in the SEM picture where the CNT-network parts that are electrically connected to the substrate are evidenced as bright structures. The bio-nanocomposite thin film has a black color due to the high concentration of carbon nanotubes loaded into the biological matrix. The porosity of the sample ensures good light penetration into the relatively thick bio-nanocomposite film. The optical transmittance (η_{tra}) of the thin film remains almost constant with values between 4 and 7% in the whole investigated near-IR range, as displayed in Figure 1d. This finding confirms the results of our previous study, which reported values of optical transparency on the same order of magnitude in the visible spectral range.[19]

DC Characteristics. In Figure 2, the current−voltage characteristics of the device based on tobacco cells and MWCNTs measured under dark conditions and under illumination are shown. The $I-V$ curves are symmetric around the origin, with a perfectly linear behavior in the investigated voltage range. Gold electrodes used for our samples have been shown to enable the realization of excellent ohmic contacts on CNT-based composite materials.[20,21] The composite film shows a low current value of 4.36×10^{-9} A at 10 V when measured under dark conditions. However, on illuminating the device with an incident light power (P_{light}) of 90 μW at 1300 nm, a change in the slope of the electrical curves, which corresponds to a resistance reduction, was noted.

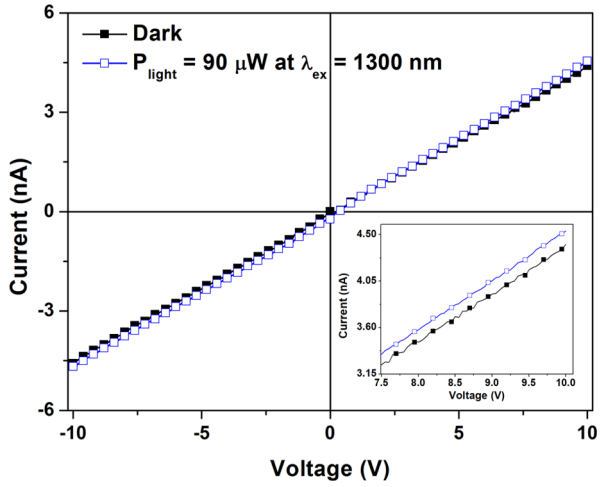

Figure 2. Current−voltage characteristics measured under dark conditions (full symbols) and under light illumination at 1300 nm with an incident optical power of 90 μW (open symbols). Inset: Difference between the $I-V$ curves, measured at different light intensities, in a restricted voltage range close to +10 V.

As clearly shown in the inset of Figure 2, the turning on of the IR light causes a slight increase of about 0.15×10^{-9} A in the current signal at 10 V. The variation in the electrical current ($\beta = \Delta I/I$) under this illumination condition is 3.4%. It is worth noting that for the illuminated sample no current has been measured without an applied voltage. The absence of any zero-bias photocurrent under illumination in our device indicates that the photovoltaic and the photothermoelectric mechanisms are negligible.[22] Therefore, the change in the electrical conductivity can be attributed either to the photoconductive or to the bolometric effect. In photoconductors, optically created electron−hole pairs are separated in the material due to an externally applied bias voltage.[22] Here, the observed resistance modulation can, most probably, be attributed to the bolometric effect, that is, to a change in the electrical conductance caused by the photoinduced heating under incident radiation.[23,24]

Temperature Dependence of the Electrical Characteristics. To investigate the influence of temperature on photoconductivity, the photoresponse of the device was measured during multiple photoswitching cycles. Under these conditions, the temperature was unregulated during the experiment, which was performed for more than 8 h overnight. The time evolution of temperature, measured during the cycles, is shown in Figure 3a (left y-axis). Here, the temperature decreases from 294.5 to 292 K for the duration

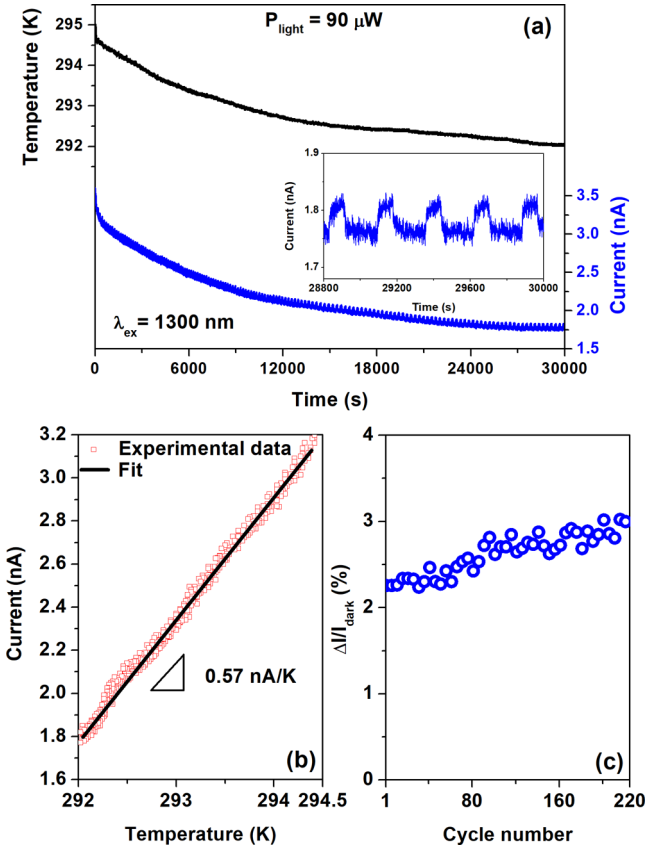

Figure 3. (a) Temperature development during the switching endurance test is shown on the left y-axis (black solid line), whereas the time evolution of the response of the photodetector at a bias voltage of +10 V, exposed to alternating dark−illumination cycles, is shown on the right y-axis (blue solid line). The inset shows a zoom into the last four cycles in the end phase of the durability test. (b) Variation of the dark current as a function of the temperature. The black solid line represents the linear fit. (c) Cycle stability of the $\Delta I/I_{dark}$ ratio measured for 220 working cycles when the device is exposed to alternating dark−illumination periods. The sensor was illuminated with a 1300 nm LED with an incident light power of 90 μW.

https://doi.org/10.1021/acsaelm.1c00368
ACS Appl. Electron. Mater. 2021, 3, 2790−2797

of the experiment. As the water content of the sample could affect the DC electrical conductivity, the weight of the device was verified before and after the experiment. Gravimetric measurements showed that only a negligible amount of water was absorbed or de-absorbed by the material during the endurance test. Therefore, no change in weight was observed. In Figure 3a (right y-axis), the current response measured over long durations of alternating dark−illumination cycles at 1300 nm (P_{light} = 90 μW) and with an applied bias voltage of 10 V is shown. As can be seen, the photoresponse exhibits a dark component (I_{dark}) that changes during the experiment following the temperature dynamics of the sample. However, the modulated current signal ($\Delta I = I - I_{dark}$) seems to be rather independent of the temperature variation of the ambient. In the inset of Figure 3a, four cycles at the final stage of the durability test are shown. When the temperature reaches a constant value (292 K), the background current remains constant and the modulated photocurrent is added to the background signal measured under dark conditions. In Figure 3b, the measured current variation as a function of the temperature is shown. As evidenced, a linear dependence of the current to the ambient temperature was observed. The best-fitting curve to the experimental data using the equation $I = I_0 + m_I (T - 293)$ is shown as the black solid line in Figure 3b. Here, I_0 is the measured current at 293 K and T is the temperature in kelvin. The resulting best-fitting parameters are as follows: I_0 = (2.4 ± 0.1) nA and m_I = (0.57 ± 0.01) nA/K. In terms of the electrical resistance, the device shows a negative temperature coefficient with a value of $m_R = -R_0 \cdot (m_I/I_0)$ of about −1 GΩ/K as displayed in Figure S1. Here, R_0 = (4.17 ± 0.08) GΩ is the corresponding resistance at 293 K. As can be observed, an increase in temperature leads to an increase in the current signal (see Figure 3b) equivalent to a decrease in the electrical resistance of the sensor. It is worth noting that m_I (or m_R) represents the sensitivity of the temperature sensor, which is the ratio between the output electrical signal I (or R) and the measured input physical parameter T.

Under dark conditions, the sample acts as a temperature sensor with a temperature coefficient of resistance (TCR) of m_I/I_0. The corresponding TCR value for our investigated sensor was 23.7%/K, which is higher than those reported in the literature for temperature sensors based on MWCNTs dispersed in different polymer matrices.[17,25−27] For example, the TCR of an epoxy/MWCNT composite, realized with the same type of MWCNT, has been reported to be only about 0.05%/K.[25] However, for pristine CNT-based devices without a polymer or epoxy matrix, TCR values of about 0.1%/K have been reported.[22,28]

In addition, the TCR absolute value at room temperature for MWCNT films was about 0.07%/K in contrast to 0.17%/K for single-walled CNT films.[28] It should also be mentioned that photoconductivity in another bio-nanocomposite material, namely, *Saccharomyces cerevisiae* yeast extract/CNT-based films, has already been observed, although only for high light intensity values.[29] To evaluate the stability of the photosensitive film, the ratio $\beta = \Delta I/I_{dark}$ was computed during the optical cycles. Figure 3c shows the $\Delta I/I_{dark}$ ratio during the 220 working cycles under operating conditions, with λ_{ex} = 1300 nm and P_{light} at 90 μW. As evidenced, good reproducibility of the current modulation induced by the light was achieved. The ratio β increases linearly from an initial value of 2.3% up to a final value of 2.9% after 220 periods. This net increment of 25% is mostly due to the reduction of the dark current by a factor of 2 with respect to its value during the first cycles. It should be noted that the current modulation ΔI, observed at the end of the durability test, is about 0.05 nA. As the investigated material is characterized by a TCR of 23.7%/K, presuming a purely bolometric effect, the change in temperature ΔT induced by light exposure can be estimated as $\Delta T = \beta/\mathrm{TCR}$. Under these conditions, a ΔT value of about 0.1 K would be expected.

To evaluate the heating effect caused by the absorbed light within the film, the measured photoresponse was correlated with the temperature dependence of the electrical characteristics by taking into account the thermal flux between the material and the ambient. Therefore, the heat balance equation under light pulse can be written as[28]

$$C\frac{\mathrm{d}\Delta T(t)}{\mathrm{d}t} = P_0 + \eta P_{light} H(t) - G\Delta T(t) \quad (1)$$

where the absorber is characterized by a heat capacity C and a thermal link by its conductivity G. The heat sink temperature is assumed to be the same as the ambient temperature, that is, 293 K. In the case of minimal reflection conditions, occurring when the incident photons are orthogonal to the sample surface, the radiation absorbance of the material $\eta \approx 1 - \eta_{tra}$ can be estimated to be 0.95. $P_0 = V_{Bias}^2/R$ is the electrical power related to the Joule self-heating and dissipated in the sample under a constant bias voltage. This latter quantity shows a value of tens of nanowatts; therefore, it can be considered to be negligible in this framework. Moreover, $H(t)$ is a rectangular pulse with $H(t)$ = 1 when the incident radiation is turned on and $H(t)$ = 0 when the incident radiation is turned off.

The solution to eq 1 is then $\Delta T(t) = \frac{\eta P_{light}}{G}(1 - e^{-t/\tau_c})$, where the temperature response changes exponentially with the thermal time constant $\tau_c = C/G$.[30] Under light illumination and stationary conditions, the thermal conductivity $G = \eta P_{light}/\Delta T$ can be computed. As the bio-nanocomposite exhibits a linear temperature dependence of the electrical characteristics $\Delta I(t) = m_I \cdot \Delta T(t)$, as displayed in Figure 3b, eq 1 can be written as

$$\Delta I(t) = m_I \frac{\eta P_{light}}{G} \cdot (1 - e^{-t/\tau_c}) \quad (2)$$

To demonstrate the thermal origin of the DC current modulation, the change in temperature on the bio-nanocomposite surface was monitored with an infrared thermometer under operating conditions during alternating dark−illumination cycles. Figure S2a,b shows the corresponding time evolutions of the temperature when the sensor was illuminated at 1300 and 780 nm with a P_{light} of 90 and 350 μW, respectively. As can be observed, the sensitive element changes its surface temperature when illuminated at different excitation wavelengths. In particular, at 1300 nm with an incident power of 90 μW, the ΔT measured 0.12 K. It should be noted that this latter value is consistent with that estimated ($\Delta T \simeq 0.1$ K) in Figure 3a with the electrical characteristics and by assuming a purely bolometric effect. However, at an excitation wavelength of 780 nm at 350 μW, the maximum temperature change measured was 0.45 K. Taking into account the solution of eq 1 in stationary conditions, the value of the thermal conductance $G = (7.5 \pm 0.2) \times 10^{-4}$ W/K can be estimated for both the wavelengths used in the reference test.

The variation in the surface temperature value monitored for both the IR wavelengths is in good agreement with the

https://doi.org/10.1021/acsaelm.1c00368
ACS Appl. Electron. Mater. 2021, 3, 2790−2797

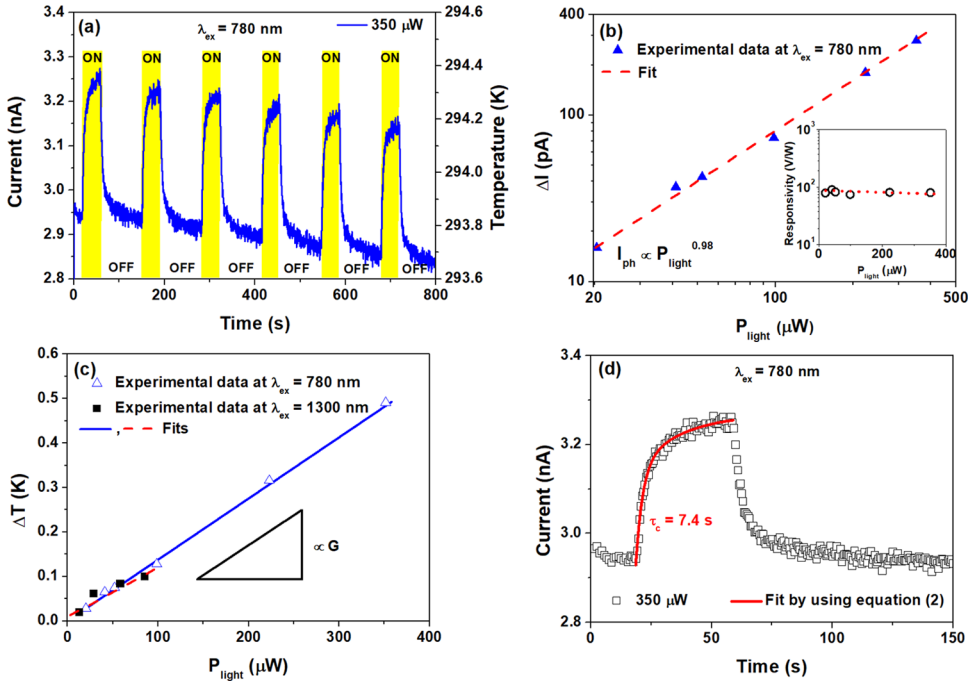

Figure 4. (a) Time evolution of the photoresponse of the bio-nanocomposite measured by applying a bias voltage of 10 V when exposed to alternating dark−illumination cycles. (b) Variation of the photocurrent as a function of the light intensity on the same device in a double logarithmic scale. The dashed line represents the best-fitting curve to the experimental data. The inset shows the voltage responsivity as a function of the incident power density at 780 nm. (c) Temperature variation induced by the absorption of the IR light at different intensities measured at 780 and 1300 nm (open triangles and filled squares, respectively). The slope of the fitting lines is related to the thermal conductivity of the bolometer close to the substrate. (d) Photocurrent transients after the switch on and switch off of the light. The red solid line is the best fit obtained using eq 2. The excitation wavelength is set to 780 nm with an incident light power of 350 μW.

assumption that the difference in the electrical characteristics under illumination can be linked to the thermal origin. This means that the change in the observed ΔI (or ΔR) could be attributed to a heating effect caused by the absorbed light. The β value estimated from Figure 3 is lower than that observed in Figure 2. This difference can be attributed to the heating effect caused by the absorption of the incident light during the long-time exposure under $I-V$ measurements. The current−voltage characteristic measurement under light illumination takes 120 s for the scan up to 10 V, and this time is sufficient to further increase the temperature of the sample, which results in an overestimation of β.

It is worth noting that the resultant bolometer based on the bio-nanocomposite tissue exhibits a TCR of about 23.7%/K; it is higher than that observed for the uncooled bolometric detection device based on vanadium oxide (~3%/K), which is the current leading platform for uncooled bolometric detection.[22,31]

Unraveling the Bolometric Effect of the Sensor Based on Tobacco Cells and MWCNTs. In Figure 4a, the time evolution of the photoresponse of the bio-nanocomposite measured at 780 nm by applying a bias voltage of 10 V in coplanar geometry is shown. The device was exposed to alternating dark−illumination cycles with an incident light intensity of 350 μW. When the device was illuminated, a clear increase in the current signal was observed. The device can be reproducibly switched between high and low conductance states. In Figure 4b, the dependence of the photocurrent on the light intensity at 780 nm is shown. Using a power-law type relationship, I_{ph} can be expressed as $I_{ph} \propto P_{light}^{\gamma}$ where $\gamma = 0.98$. The monotonic variation of the photocurrent for different light power values ranging from 10 to 400 μW indicates a good sensitivity for the temperature sensor. The photocurrent was linearly proportional to the light intensity, reaching a value of 280 pA at the maximum incident optical power. The current modulation was also observed for other wavelengths in the visible range (e.g., 400 and 660 nm), as displayed in Figure S3.

As evidenced, the corresponding value of the current responsivity $\mathcal{R}_i = I_{ph}/P_{light}$ of the photoreceiver based on tobacco cells and MWCNTs at 780 nm was 0.85 μA/W for the whole investigated range of P_{light}. As the device is voltage biased, the voltage responsivity can be evaluated as $\mathcal{R}_v = \mathcal{R}_i \times R_s$.[32]

Here, R_s = 100 MΩ is the internal electrical resistance of the source measurement unit. The resulting value of $\mathcal{R}_v$ is 85 V/W. Several authors have reported the value of $\mathcal{R}_v$ on the same order of magnitude (30 − 150 V/W) for bolometers fabricated with nanocomposite materials incorporating carbon nanotubes.[15,33−35] It should be noted that Simmons et al. prepared a composite film for bolometric applications based on a conductive ink with single-walled CNTs having a TCR value of about −6.5%/K and a voltage responsivity $\mathcal{R}_v$ of about 50 V/W.[36] In the inset of Figure 4b, the $\mathcal{R}_v$ values as a function of the incident light power are shown. As can be noted, the responsivity is almost constant as a function of P_{light}, showing a stable operating condition of the device. To determine the G value of the unsuspended temperature sensor, associated with the thermal link with the substrate, the temperature variations $\Delta T = \eta P_{light}/G$ measured as a function of different light intensities at 780 and 1300 nm have been taken into account. In stationary conditions, the linear slope, observed in the experimental data displayed in Figure 4c, is related to the

https://doi.org/10.1021/acsaelm.1c00368
ACS Appl. Electron. Mater. 2021, 3, 2790−2797

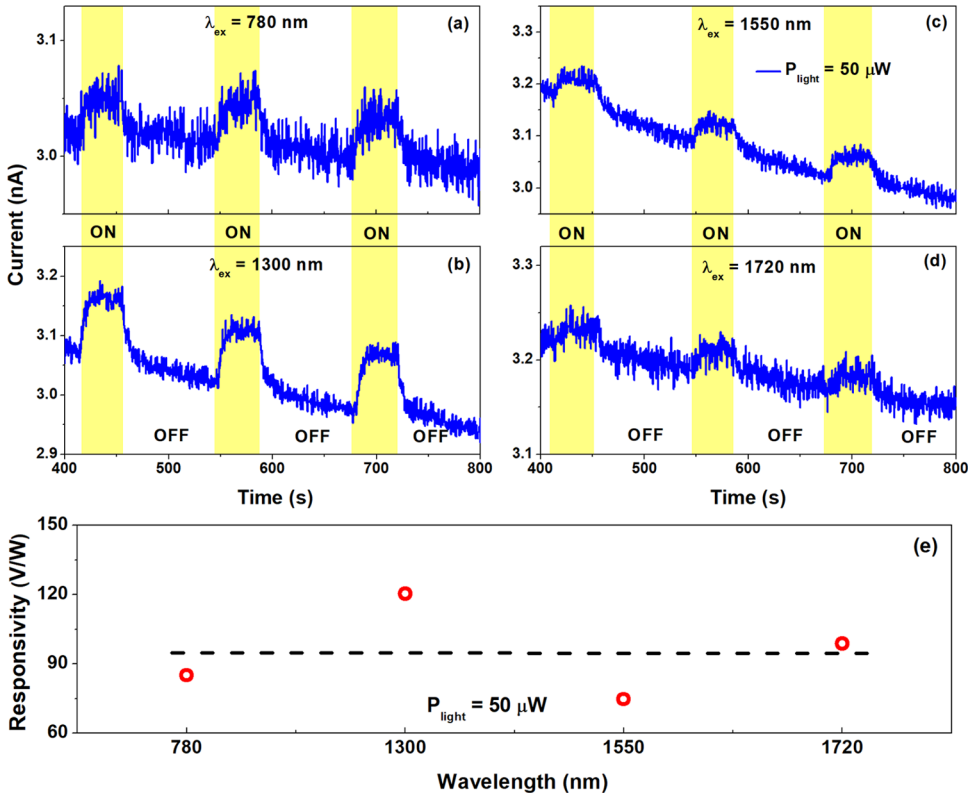

Figure 5. Time evolutions of the photoresponse of the bio-nanocomposite measured at a bias voltage of 10 V when exposed to alternating dark–illumination cycles at λ_{ex} of (a) 780 nm, (b) 1300 nm, (c) 1550 nm, and (d) 1720 nm. (e) Voltage responsivity of the thin film in the investigated near-infrared range. The dashed line represents the average value of $\mathcal{R}_v$. The incident light power is 50 μW.

thermal conductivity value of the device that works as a bolometer. It should be noted that the G value estimated for the bio-nanocomposite, when exposed to an IR excitation at 780 nm, is $G = (6.8 \pm 0.2) \times 10^{-4}$ W/K. Moreover, the value computed for λ_{ex} at 1300 nm is $G = (8.9 \pm 0.2) \times 10^{-4}$ W/K, consistent with that estimated in Figure S2. Here, the G value computed for both the excitation wavelengths are quite similar to the ones evaluated in the reference tests. This finding demonstrates that the thermal link of the measuring setup, displayed in Figure 1b, remains the same in all performed experiments. In the literature, several authors have reported G values lower than two orders of magnitude for highly performing bolometers.[22,35] This difference is essentially due to the thermal link of the sample with the ambient for the investigated multifunctional sensor device in the unsuspended state. In Figure 4d, the time evolution of the photocurrent response during one alternating dark–illumination cycle is shown. Rise time is defined as the time interval from 10 to 90% of the saturated photocurrent with respect to the dark current after the light is switched on. During this single cycle, the ambient temperature can be considered constant, as observed by the steady value of the background current for the entire time considered.

To evaluate the dynamics of the phototransients, a fitting procedure was performed using an exponential growth function, described in eq 2. In Figure 4d, the transients of the current signal, the best-fitting curve, and the resulting time constant value τ_c are shown. As evidenced, the fit procedure gives the τ_c value on the time scale of seconds. The response time of the temperature sensor is much slower than that reported in the literature for infrared bolometers based on carbon nanotube/polymer composites.[22,37,38] In this proof of concept, the investigated multifunctional sensor has a large area and a thickness of more than 100 μm, which increases the heat transfer within the material. Moreover, the device under the operating conditions is unsuspended and this increases the rise time of the sensor. To enhance the speed of this bolometer-type sensor to as low as fractions of a second, the geometry of the sample (thickness and active area) has to be optimized.[15] However, device optimization is out of the scope of this work and will be the subject of future research. Once the device is illuminated with a λ_{ex} = 780 nm at 350 μW, the electrical resistance varies with the temperature rise owing to the absorption of the incoming electromagnetic radiation. Therefore, the current signal exponentially increases reaching a steady-state value of about 3.25 nA equivalent to an increment of the temperature within the absorber material of about 0.5 K. It should be noted that this value, estimated from the photoresponse characteristics of the device, is similar to that measured during the reference test with the IR thermometer in Figure S2b. By switching off the excitation, the whole system will slowly return to its original thermal equilibrium state, showing a current value similar to that observed under dark conditions. When the device is not illuminated, it works as a temperature sensor showing a background current I_{dark} of about 2.95 nA corresponding to a temperature of 20.8 °C, as displayed in Figure 3b.

To evaluate the response of the material to different wavelengths in the near-infrared region, the device was exposed to light excitation at 780, 1300, 1550, and 1720 nm. In this case, for comparison, the constant optical power of the LED light of 50 μW was chosen. In Figure 5, the time

https://doi.org/10.1021/acsaelm.1c00368
ACS Appl. Electron. Mater. 2021, 3, 2790–2797

evolutions of the photoresponse for illumination with different wavelengths, all measured at a bias voltage of 10 V, during alternating dark−illumination cycles having a period of about 120 s are shown. As evidenced, an increase in the current signal was observed when the excitation was turned on for all of the investigated wavelengths. Moreover, once the illumination was switched off, a slower decay was noted. Again, the thermal conductivity between the sensor and the substrate and the large heat capacity, due to the nonoptimized geometry of the sensor, influence the response time of the bolometer. In Figure 5e, the responsivity values as a function of the excitation wavelengths for a constant optical power of 50 μW are reported. On increasing λ_{ex}, the responsivity of the device increased showing a maximum value of about 120 V/W at 1300 nm. Subsequently, $\mathcal{R}_v$ decreased, reaching a value of about 98 V/W at 1720 nm. The multifunctional sensor exhibits an average value of voltage responsivity of 95.2 ± 2.2 V/W for all of the investigated telecom wavelengths in the near-infrared range. It is also worth noting that in the technologically important NIR range beyond 1100 nm, which is not covered by conventional silicon photodiodes, a rather high responsivity was achieved. Moreover, a thermal photodetector that can operate at room temperature without the need for cooling is highly desirable.[14]

CONCLUSIONS

The application of a highly temperature-sensitive bio-nano tissue, realized with tobacco cells as the matrix and multiwalled carbon nanotubes as fillers at room temperature, as an NIR bolometer was demonstrated. The initially relatively high conductivity of the as-deposited nanomaterial was lost in a high-voltage burn-in procedure, which interrupted the continuous nanotube conduction paths and lowered the dark conductivity by some orders of magnitude. The electrical conductivity of the resulting device, finished by the evaporation of lateral coplanar gold contacts, strongly increased with increasing temperature, which was reversible for small temperature excursions around room temperature and extremely sensitive to light. Here, the operation as a light sensor at room temperature under irradiation with low-intensity light between 780 and 1720 nm is demonstrated. This means that it can also be applied in the technologically important wavelength ranges of around 1300 and 1550 nm, which is not covered by conventional low-cost silicon photodiodes. A bolometer-type operation principle is consistent with the determined temperature sensitivity and time response of the light sensor.

ASSOCIATED CONTENT

Supporting Information

The Supporting Information is available free of charge at https://pubs.acs.org/doi/10.1021/acsaelm.1c00368.

Variation of the resistance measured under dark conditions as a function of temperature; cycle stability when the device is exposed to alternating dark−illumination cycles; and time evolutions of the surface temperature, measured during the reference test, for different excitation wavelengths (PDF)

AUTHOR INFORMATION

Corresponding Author

Giovanni Landi − *ENEA, Portici Research Center, 80055 Portici, NA, Italy; Department of Industrial Engineering (DIIn), Salerno University, 84084 Fisciano, SA, Italy;* orcid.org/0000-0002-0640-479X; Email: giovanni.landi@enea.it

Author

Heinz-Christoph Neitzert − *Department of Industrial Engineering (DIIn), Salerno University, 84084 Fisciano, SA, Italy*

Complete contact information is available at: https://pubs.acs.org/10.1021/acsaelm.1c00368

Notes

The authors declare no competing financial interest.

ACKNOWLEDGMENTS

The bio-nano tissue was realized in a wide collaboration by researchers, all from Salerno University, who came either from the Department of Pharmacy or from the Department of Industrial Engineering. For a complete list of the involved researchers, the reader is referred to a previous publication.[17] For the sample processing with a focused ion beam tool and the subsequent scanning electron microscopy imaging of the sensor material, the authors thank Prof. C. Boit and H. Wegner from the Institute of Semiconductor Devices of the Technical University Berlin.

REFERENCES

(1) Xu, K.; Lu, Y.; Takei, K. Multifunctional Skin-Inspired Flexible Sensor Systems for Wearable Electronics. *Adv. Mater. Technol.* **2019**, *4*, No. 1800628.

(2) Nakata, S.; Arie, T.; Akita, S.; Takei, K. Wearable, Flexible, and Multifunctional Healthcare Device with an ISFET Chemical Sensor for Simultaneous Sweat PH and Skin Temperature Monitoring. *ACS Sens.* **2017**, *2*, 443−448.

(3) Xie, M.; Hisano, K.; Zhu, M.; Toyoshi, T.; Pan, M.; Okada, S.; Tsutsumi, O.; Kawamura, S.; Bowen, C. Flexible Multifunctional Sensors for Wearable and Robotic Applications. *Adv. Mater. Technol.* **2019**, *4*, No. 1800626.

(4) Lin, C.; Xian, X.; Qin, X.; Wang, D.; Tsow, F.; Forzani, E.; Tao, N. High Performance Colorimetric Carbon Monoxide Sensor for Continuous Personal Exposure Monitoring. *ACS Sens.* **2018**, *3*, 327−333.

(5) Pfattner, R.; Lebedev, V.; Laukhina, E.; Kumar, S. C.; Esteban-Martin, A.; Ramaiah-Badarla, V.; Ebrahim-Zadeh, M.; de Arquer, F. P. G.; Konstantatos, G.; Laukhin, V.; Rovira, C.; Veciana, J. A Highly Sensitive Pyroresistive All-Organic Infrared Bolometer. *Adv. Electron. Mater.* **2015**, *1*, No. 1500090.

(6) Runowski, M.; Shyichuk, A.; Tymiński, A.; Grzyb, T.; Lavín, V.; Lis, S. Multifunctional Optical Sensors for Nanomanometry and Nanothermometry: High-Pressure and High-Temperature Upconversion Luminescence of Lanthanide-Doped Phosphates—$LaPO_4$ /YPO_4:Yb^{3+} −Tm^{3+}. *ACS Appl. Mater. Interfaces* **2018**, *10*, 17269−17279.

(7) Tan, C. L.; Mohseni, H. Emerging Technologies for High Performance Infrared Detectors. *Nanophotonics* **2018**, *7*, 169−197.

(8) Zhao, X.-H.; Ma, S.-N.; Long, H.; Yuan, H.; Tang, C. Y.; Cheng, P. K.; Tsang, Y. H. Multifunctional Sensor Based on Porous Carbon Derived from Metal−Organic Frameworks for Real Time Health Monitoring. *ACS Appl. Mater. Interfaces* **2018**, *10*, 3986−3993.

(9) Song, M.; Seo, J.; Kim, H.; Kim, Y. Ultrasensitive Multi-Functional Flexible Sensors Based on Organic Field-Effect Transistors

with Polymer-Dispersed Liquid Crystal Sensing Layers. *Sci. Rep.* **2017**, *7*, No. 2630.
(10) Petritz, A.; Wolfberger, A.; Fian, A.; Griesser, T.; Irimia-Vladu, M.; Stadlober, B. Cellulose-Derivative-Based Gate Dielectric for High-Performance Organic Complementary Inverters. *Adv. Mater.* **2015**, *27*, 7645−7656.
(11) Dincer, C.; Bruch, R.; Costa-Rama, E.; Fernández-Abedul, M. T.; Merkoçi, A.; Manz, A.; Urban, G. A.; Güder, F. Disposable Sensors in Diagnostics, Food, and Environmental Monitoring. *Adv. Mater.* **2019**, No. 1806739.
(12) Landi, G.; Sorrentino, A.; Fedi, F.; Neitzert, H. C.; Iannace, S. Cycle Stability and Dielectric Properties of a New Biodegradable Energy Storage Material. *Nano Energy* **2015**, *17*, 348−355.
(13) Landi, G.; Sorrentino, A.; Iannace, S.; Neitzert, H. C. Differences between Graphene and Graphene Oxide in Gelatin Based Systems for Transient Biodegradable Energy Storage Applications. *Nanotechnology* **2017**, *28*, No. 054005.
(14) Sassi, U.; Parret, R.; Nanot, S.; Bruna, M.; Borini, S.; De Fazio, D.; Zhao, Z.; Lidorikis, E.; Koppens, F. H. L.; Ferrari, A. C.; Colli, A. Graphene-Based Mid-Infrared Room-Temperature Pyroelectric Bolometers with Ultrahigh Temperature Coefficient of Resistance. *Nat. Commun.* **2017**, *8*, No. 14311.
(15) Håkansson, A.; Shahi, M.; Brill, J. W.; Fabiano, S.; Crispin, X. Conducting-Polymer Bolometers for Low-Cost IR-Detection Systems. *Adv. Electron. Mater.* **2019**, *5*, No. 1800975.
(16) Nagata, T.; Nemoto, Y.; Hasezawa, S. Tobacco BY-2 Cell Line as the "HeLa" Cell in the Cell Biology of Higher Plants. In *International Review of Cytology*; Academic Press, 1992; Vol. *132*, pp 1−30.
(17) Di Giacomo, R.; Maresca, B.; Angelillo, M.; Landi, G.; Leone, A.; Vaccaro, M. C.; Boit, C.; Porta, A.; Neitzert, H. C. Bio-Nano-Composite Materials Constructed With Single Cells and Carbon Nanotubes: Mechanical, Electrical, and Optical Properties. *IEEE Trans. Nanotechnol.* **2013**, *12*, 1026−1030.
(18) Liparoti, S.; Landi, G.; Sorrentino, A.; Speranza, V.; Cakmak, M.; Neitzert, H. C. Flexible Poly(Amide-Imide)-Carbon Black Based Microheater with High-Temperature Capability and an Extremely Low Temperature Coefficient. *Adv. Electron. Mater.* **2016**, *2*, No. 1600126.
(19) Neitzert, H. C.; Landi, G.; Chiadini, F.; Knez, M.; Lakhtakia, A.; Martín-Palma, R. J. Sensitive Photoreceiver Based on Carbon Nanotube/Tobacco Cell Composite Material, In *Proceedings of SPIE - The International Society for Optical Engineering*, 2017; p 1016210.
(20) Neitzert, H. C.; Landi, G. Influence of the Contact Metallization on the Characteristics of Resistive Temperature Sensors Based on EPOXY/MWCNT Composites. In *Sensors: Proceedings of the Second National Conference on Sensors*, (Rome 19-21 February, 2014); Compagnone, D.; Baldini, F.; Di Natale, C.; Betta, G.; Siciliano, P., Eds.; Springer International Publishing: Cham, 2015; pp 333−337.
(21) Zhang, T.-F.; Li, Z.-P.; Wang, J.-Z.; Kong, W.-Y.; Wu, G.-A.; Zheng, Y.-Z.; Zhao, Y.-W.; Yao, E.-X.; Zhuang, N.-X.; Luo, L.-B. Broadband Photodetector Based on Carbon Nanotube Thin Film/Single Layer Graphene Schottky Junction. *Sci. Rep.* **2016**, *6*, No. 38569.
(22) He, X.; Léonard, F.; Kono, J. Uncooled Carbon Nanotube Photodetectors. *Adv. Opt. Mater.* **2015**, *3*, 989−1011.
(23) Low, T.; Engel, M.; Steiner, M.; Avouris, P. Origin of Photoresponse in Black Phosphorus Phototransistors. *Phys. Rev. B* **2014**, *90*, No. 081408.
(24) Richards, P. L. Bolometers for Infrared and Millimeter Waves. *J. Appl. Phys.* **1994**, *76*, 1−24.
(25) Neitzert, H. C.; Vertuccio, L.; Sorrentino, A. Epoxy/MWCNT Composite as Temperature Sensor and Electrical Heating Element. *IEEE Trans. Nanotechnol.* **2011**, *10*, 688−693.
(26) Barone, C.; Landi, G.; Mauro, C.; Neitzert, H. C.; Pagano, S. Universal Crossover of the Charge Carrier Fluctuation Mechanism in Different Polymer/Carbon Nanotubes Composites. *Appl. Phys. Lett.* **2015**, *107*, No. 143106.
(27) Nobile, M. R.; Valentino, O.; Morcom, M.; Simon, G. P.; Landi, G.; Neitzert, H.-C. The Effect of the Nanotube Oxidation on the Rheological and Electrical Properties of CNT/HDPE Nanocomposites. *Polym. Eng. Sci.* **2017**, *57*, 665−673.
(28) Lu, R.; Shi, J. J.; Baca, F. J.; Wu, J. Z. High Performance Multiwall Carbon Nanotube Bolometers. *J. Appl. Phys.* **2010**, *108*, No. 084305.
(29) Valentini, L.; Bon, S. B.; Signetti, S.; Tripathi, M.; Iacob, E.; Pugno, N. M. Fermentation Based Carbon Nanotube Multifunctional Bionic Composites. *Sci. Rep.* **2016**, *6*, No. 27031.
(30) Rieke, G. *Detection of Light*; Cambridge University Press: Cambridge, 2002, pp 238−274.
(31) Yuan, S.; Yu, R.; Ma, C.; Deng, B.; Guo, Q.; Chen, X.; Li, C.; Chen, C.; Watanabe, K.; Taniguchi, T.; García de Abajo, F. J.; Xia, F. Room Temperature Graphene Mid-Infrared Bolometer with a Broad Operational Wavelength Range. *ACS Photonics* **2020**, *7*, 1206−1215.
(32) Dillner, U.; Kessler, E.; Meyer, H.-G. Responsivity and Detectivity Modelling of Thermal Radiation Sensors Based on a Biased Thermocouple. *J. Phys. D: Appl. Phys.* **2011**, *44*, No. 305102.
(33) Vera-Reveles, G.; Simmons, T. J.; Bravo-Sánchez, M.; Vidal, M. A.; Navarro-Contreras, H.; González, F. J. High-Sensitivity Bolometers from Self-Oriented Single-Walled Carbon Nanotube Composites. *ACS Appl. Mater. Interfaces* **2011**, *3*, 3200−3204.
(34) Glamazda, A. Y.; Karachevtsev, V. A.; Euler, W. B.; Levitsky, I. A. Achieving High Mid-IR Bolometric Responsivity for Anisotropic Composite Materials from Carbon Nanotubes and Polymers. *Adv. Funct. Mater.* **2012**, *22*, 2177−2186.
(35) John, J.; Muthee, M.; Yogeesh, M.; Yngvesson, S. K.; Carter, K. R. Suspended Multiwall Carbon Nanotube-Based Infrared Sensors via Roll-to-Roll Fabrication. *Adv. Opt. Mater.* **2014**, *2*, 581−587.
(36) Simmons, T. J.; Vera-Reveles, G.; González, G.; Gutiérrez-Hernández, J. M.; Linhardt, R. J.; Navarro-Contreras, H.; González, F. J. Bolometric Properties of Semiconducting and Metallic Single-Walled Carbon Nanotube Composite Films. *ACS Photonics* **2015**, *2*, 334−340.
(37) Pradhan, B.; Setyowati, K.; Liu, H.; Waldeck, D. H.; Chen, J. Carbon Nanotube−Polymer Nanocomposite Infrared Sensor. *Nano Lett.* **2008**, *8*, 1142−1146.
(38) Pradhan, B.; Kohlmeyer, R. R.; Setyowati, K.; Owen, H. A.; Chen, J. Advanced Carbon Nanotube/Polymer Composite Infrared Sensors. *Carbon* **2009**, *47*, 1686−1692.

https://doi.org/10.1021/acsaelm.1c00368
ACS Appl. Electron. Mater. 2021, 3, 2790−2797